IEEE Access
Multidisciplinary | Rapid Review | Open Access Journal

Received October 3, 2019, accepted November 21, 2019, date of publication December 3, 2019, date of current version December 26, 2019.

Digital Object Identifier 10.1109/ACCESS.2019.2957419

Quadrature Index Modulation With Three-Dimension Constellation

FUCHUN HUANG[1,3], XUEHUA LIU[1], ZHILI ZHOU[2], JIABING LUO[1], AND JILIN WANG[1]

[1]Department of Computer, South China Institute of Software Engineering, Guangzhou 510990, China
[2]College of Electrical and Electronic Engineering, Wenzhou University, Wenzhou 325035, China
[3]School of Electronic and Information Engineering, Sun Yat-sen University, Guangzhou 510275, China

Corresponding author: Zhili Zhou (zhouzhili@wzu.edu.cn)

This work was supported in part by Foundation for Young Talents in Higher Education of Guangdong (N. 2018KQNCX390) and in part by Wenzhou Science and Technology Project (N. 2018N0042).

ABSTRACT Quadrature spatial modulation (QSM) is a novel index modulation technology, which extends the antenna index (AI) to two dimensions of both in-phase AI and quadrature AI. In order to further make full use of the idle transmit antennas (TAs) resource and to exploit the signal constellation domain, taking advantage of the spatial dimension of QSM, we propose a new three-dimension (3D) structure of quadrature index modulation (QIM), which is capable of not only transmitting directly a 3D constellation symbol but also carrying more extra information bits, named as quadrature index modulation with three-dimensional constellation (QIM-TDC). More specifically, a 3D framework of QIM-TDC is designed for transmitting a 3D constellation symbol that is constructed by the X-axis, Y-axis and Z-axis components. In the proposed QIM-TDC scheme, by utilizing an in-phase AI vector, two active TAs are activated simultaneously to transmit the X-axis and Y-axis components of the 3D symbol, respectively. Similarly, by utilizing the quadrature AI vector, an active TA is activated to transmit the Z-axis component of the 3D symbol. Then, for further achieving the better bit error probability (BEP) performance, the design of a modified 3D constellation for maximizing the squared minimum Euclidean distance (MED) between the transmitted spatial vectors (TSVs) is illustrated. Moreover, the squared MEDs for QIM-TDC are analyzed and compared with the squared MEDs of the conventional spatial modulation schemes. Finally, The average BEP is analyzed in this paper. Numerical results with comparison among the other schemes demonstrate the QIM-TDC scheme achieves the improved performance.

INDEX TERMS Quadrature index modulation with three-dimensional constellation (QIM-TDC), three dimension (3D) constellation, 3D framework, squared minimum Euclidean distance (MED), transmitted spatial vector (TSV).

I. INTRODUCTION

Index modulation [1] technologies such as spatial modulation (SM) [2], [3] and the extension of SM called quadrature spatial modulation (QSM) [4] have wisely attracted researchers' attention due to the activation of transmit antennas (TAs) by exploiting the spatial domain. One of the objectives of using these technologies is to transmit extra information bits being used for the indexes of active antenna(s).

To exploit the potential gain from the spatial domain of TAs, on the one hand, by the index modulation technology of SM, a number of improved schemes on SM with multiple active TAs [5]–[9] has been developed not only for solving the shortcoming of the single radio frequency (RF)-chain constraint in SM but also for transmitting more extra information bits compared with SM. Furthermore, a generalized SM (GSM) reported in [5], [6] achieves the spatial diversity gain by transmitting an identical quadrature amplitude modulation or phase shift modulation (QAM/PSK) symbol through multiple active TAs at one time slot. Nevertheless, the multiple active TAs reported in [7]–[9] are used to transmitting different QAM/PSK symbols not only for enhancing high spectral efficiency but also achieving the spatial multiplexing gain. On the other hand, by the index modulation technology of QSM, double spatial modulation (DSM) [10], with the aid

The associate editor coordinating the review of this manuscript and approving it for publication was Ke Guan.

of a rotation angle, directly superimposes two independently SM transmit vectors for the transmission of high data rate.

In high signal noise ratio (SNR) region, the average bit error probability (BEP) is mainly determined by the worst pairwise error probability (PEP), which corresponds to the crucial parameter of the squared minimum Euclidean distane (MED) between the transmitted spatial vectors (TSVs) that is constructed by both the conventional QAM/PSK symbol(s) and the indexes of active antenna(s). To exploit the potential gain from the signal constellation domain, a lot of researches on optimizing design of signal constellation (i.e. Amplitude/phase modulation (APM) and star-quadrature amplitude modulation) have been reported in [11]–[14]. Consequently, the BEP performance of the SM system can be further improved due to the increasing of the squared MED between the TSVs. In [15], the in-phase and quadrature components of APM symbols, which are dependent on the TA, are optimized for increasing the squared MED the TSVs. Furthermore, enhanced SM (ESM) reported in [16], [17] is proposed to transmit one primary symbol (e.g. M-ary QAM) by using one active TA or to transmit two secondary symbols by using two active TAs during each time slot. Through considering the combination of active TA(s) and signal constellation design, the key idea of ESM is to enhance the transmission of extra information bits by extending the number of the indexes of active TA(s) and to increase the squared MED between the TSVs for the better BEP performance.

In brief, the objective of designing on signal constellation or of being capable of carrying more extra antenna index (AI) bits is to maximize the squared MED between the TSVs for the improving of BEP performance.

Against this background, to the best of our knowledge, no work regarding the amalgamation of index modulation technology and three dimension (3D) constellation is available in the literature. In this paper, we propose a new 3D framework of quadrature index modulation used to transmit a 3D constellation symbol, named as quadrature index modulation with 3D constellation (QIM-TDC).

The main contributions of this paper are as follows:

1) The 3D framework of the QIM-TDC scheme is developed, which can transmit directly a 3D constellation symbol by using the in-phase and quadrature spatial dimensions.
2) In the proposed QIM-TDC scheme, in order to make trade-off between the multiplexing and diversity gain and to enhance the transmission of higher spectral efficiency. The X-axis, Y-axis and Z-axis components of a 3D constellation symbol are transmitted by the following methods. (a). Two active antennas in in-phase spatial dimension are activated by the in-phase AI vector to transmit respectively the X-axis and Y-axis components of the 3D constellation symbol, resulting in an in-phase spatial constellation. (b). One active antenna in quadrature spatial dimension is activated by the quadrature AI vector to transmit the remaining one Z-axis component of the 3D constellation symbol, resulting in a quadrature constellation. Then a TSV symbol is constructed by adding the in-phase and quadrature spatial constellations.
3) By exploiting the spatial gain from the signal constellation domain, a modified 3D constellation is designed for further increasing the squared MED between the TSVs according to the trait of the squared MED between the TSVs.
4) The squared MEDs of the QIM-TDC scheme compared with that of other MIMO schemes (such as SM, QSM, ESM) are made detailed analysis and the average BEP is derived based on the union bound technique.

TABLE 1. List of notations.

N_t	Number of transmit antennas
N_r	Number of receive antennas
Ω_s	QAM/PSK signal set
Ω_S	3D signal set
$s_{\mathfrak{R}}^{\mathrm{Q}}$	Real part of QAM signal point
$s_{\mathfrak{I}}^{\mathrm{Q}}$	Imaginary part of QAM signal point
s^{P}	Signal point of PAM
$\tilde{s}^{\mathrm{P}}$	Signal point of modified PAM
$E_{\mathrm{av}}^{\mathrm{3D}}$	Average energy per traditional 3D signal point
$\tilde{E}_{\mathrm{av}}^{\mathrm{3D}}$	Average energy per modified 3D signal point
$d_{\mathbf{S},\min}^2$	Euclidean distance between the TSVs
$\tilde{d}_{\mathbf{S},\min}^2$	Squared MED between the TSVs
TSV	Transmitted spatial vector
MED	Minimum Euclidean distance
TA	Transmit antenna
AI	Antenna index
3DCI	Traditional 3D constellation
3DCII	Modified 3D constellation
QIM-TDCI	QIM-TDC with 3DCI constellation
QIM-TDCII	QIM-TDC with 3DCII constellation

The rest of this paper are organized as below. Section II briefly introduces the related research works on both SM and QSM schemes. Then, Section III describes the details of the QIM-TDC scheme. A new 3D construction of constellation is designed in Section IV. Moreover, the squared MED and the theoretical analysis of QIM-TDC are performed in Section V, and the simulation results are given in Sections VI. Finally, VII concludes this paper.

The notations for various system parameters and acronyms used throughout the paper are listed in Table 1

II. RELATED WORKS

For the SM technology [2], it conveys the information bits not only by the data symbols (e.g. QAM/PSK), but also by the antenna indexes of activating one out of TAs. Compared with the vertical Bell Labs layered space-time (V-BLAST) [18] scheme, SM can significantly combat the inter-channel interference and reduce the complexity of detection at the receiver. For the QSM [4] technology, since QSM extends the spatial constellation of SM to the in-phase and quadrature index dimensions, it gains the additional information bits with base-two logarithm of the number of TAs compared with SM.

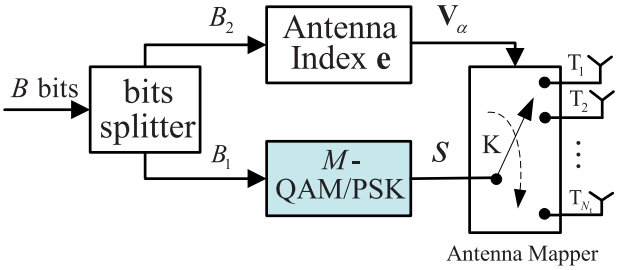

FIGURE 1. System Model of the SM system.

In this paper, the design concept of QIM-TDC is inspired from the SM and QSM systems. The 3D framework of the QIM-TDC system with 3D constellation is designed for the achievable spatial gain from the spatial and signal constellation domains and is the extension of the spatial dimensions of the QSM system with 2D constellation for the transmission of both more extra information bits and higher dimensional constellation. In our proposed QIM-TDC, a 3D symbol from a 3D constellation set Ω_S is directly transmitted from the corresponding active TAs without converting 3D constellation into 2D constellation. Furthermore, the in-phase index dimension of QSM is extended into two in-phase index dimensions for the transmission of two components of a 3D symbol on two active TAs. Due to the activation of two TAs, QSM-TDC not only extends the number of the in-phase AI vectors for the selection of the in-phase AI information bits but also make fully the idle TAs resource. Therefore, at the beginning of designing the QIM-TDC system, we briefly introduce two traditional spatial modulation schemes such as SM and QSM constituting the design basis of our proposed scheme.

A. SM SCHEME

In the SM scheme [2] with N_t TAs, as shown in Fig. 1, $B = \log_2 M + \log_2 N_t$ bits are conveyed by both the antenna index (AI) modulator and a M-QAM/PSK module, where M denotes the number of the constellation points (CPs). Compared with the single-input multiple-output (SIMO) system using the same M-QAM/PSK, the SM system can achieve higher throughput of $\log_2 N_t$ bits since the spatial domain of TAs is exploited at cost of building multiple TAs.

The working principle of the transmitter in the SM system is as follows: the entering bit stream of B bits are first divided into two blocks of both $B_1 = \log_2 M$ bits and $B_2 = \log_2 N_t$ bits. Then an AI vector $\mathbf{V}_\alpha$ obtained by mapping the B_2 bits is used to activate one out of N_t TAs, where $\mathbf{V}_\alpha \in \mathbf{R}^{N_t}, \alpha = 1, 2, \cdots, N_t$, is the α-th column of the $(N_t \times N_t)$-element identity matrix $\mathbf{I}_{N_t}$. In other words, only a single RF-chain TA is activated to transmit a M-QAM/PSK symbol s from a M-ary constellation set Ω_s, which is obtained by modulating B_1 bits, namely the N_t of spatial index vectors for the transmitted spatial vectors (TSVs) with the dimension of $N_t \times 1$, which correspond to a CP symbol s, is obtained by the modulated symbol s multiplied by the AI vector $\mathbf{V}_\alpha$ as

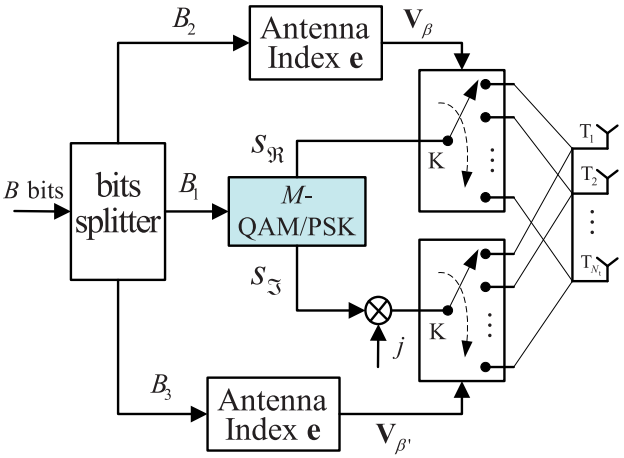

FIGURE 2. System model of the QSM system.

below

$$\mathbf{S}_{\mathrm{SM}} \in \left\{ \begin{bmatrix} s \\ 0 \\ \vdots \\ 0 \end{bmatrix}_{N_t \times 1}, \begin{bmatrix} 0 \\ s \\ \vdots \\ 0 \end{bmatrix}_{N_t \times 1}, \cdots, \begin{bmatrix} 0 \\ 0 \\ \vdots \\ s \end{bmatrix}_{N_t \times 1} \right\} \tag{1}$$

Note that N_t need to satisfy the power of 2, s denotes one CP from M-ary constellation set Ω_s.

Thus, the squared MED between the TSVs could be calculated by

$$d^2_{\mathbf{S}_{\mathrm{SM}},\min} = \min_{\mathbf{S}_{\mathrm{SM}} \neq \tilde{\mathbf{S}}_{\mathrm{SM}}} \left\{ \left\| \mathbf{S}_{\mathrm{SM}} - \tilde{\mathbf{S}}_{\mathrm{SM}} \right\|^2 \right\} = \frac{4}{E_{\mathrm{av}}} \tag{2}$$

where E_{av} denotes the average energy of each CP in M-QAM/PSK constellation.

B. QSM SCHEME

An extension of SM is the QSM system [4] with N_t TAs, as shown in Fig. 2. The $B = \log_2 M + \log_2 N_t^2$ bits are conveyed by two AI modules and a M-QAM/PSK modulator. Compared with the SM system, one more antenna index mapper is considered for the QSM system, implying that the QSM system can achieves one more additional $\log_2 N_t$ information bits not only by exploiting the signal constellation domain, but also by extending the spatial domain without increasing the number of TAs and the detection complexity at the receiver.

The working principle of the transmitter in the QSM system is as follows: in Fig. 2, the entering bit stream of B bits are divided into three blocks of $B_1 = \log_2 M$ bits, $B_2 = \log_2 N_t$ bits and $B_3 = \log_2 N_t$ bits. B_1 bits are first modulated into a M-QAM/PSK symbol s from a M-ary constellation set Ω_s. Furthermore, the modulated symbol s is divided into two parts of the in-phase component $s_\Re$ and the quadrature component $s_\Im$. Then, the active TA activated by the AI vector $\mathbf{V}_\beta$, which is obtained by mapping B_2 bits, is used to transmit the in-phase component $s_\Re$, resulting in the in-phase spatial index vector $s_\Re \cdot \mathbf{V}_\beta$. The active TA activated

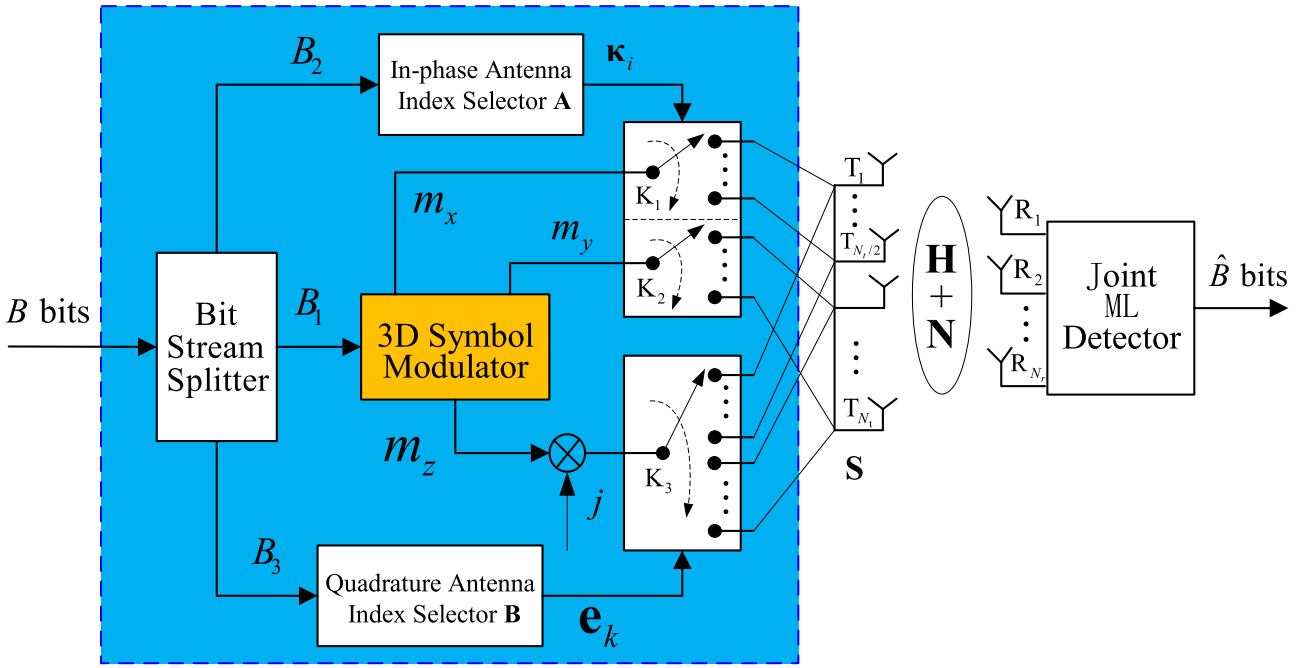

FIGURE 3. System model of the QIM-TDC system.

by the AI vector $\mathbf{V}_{\beta'}$, which is obtained by mapping B_3 bits, is used to transmit the quadrature component $s_{\Im}$, resulting in the quadrature spatial index vector $s_{\Im} \cdot \mathbf{V}_{\beta'}$.

Consequently, by adding the in-phase and quadrature spatial index vectors, the N_t^2 spatial vectors for the TSVs, which correspond to a CP symbol s, may be expressed as below

$$\mathbf{S}_{\mathrm{QSM}} \in \left\{ \begin{bmatrix} s \\ 0 \\ \vdots \\ 0 \end{bmatrix}_{N_t \times 1}, \begin{bmatrix} s_{\Re} \\ j s_{\Im} \\ \vdots \\ 0 \end{bmatrix}_{N_t \times 1}, \cdots, \begin{bmatrix} 0 \\ 0 \\ \vdots \\ s \end{bmatrix}_{N_t \times 1} \right\} \quad (3)$$

It can be seen from (3) that QSM need $\log_2 N_t^2$ extra index bits to modulate N_t^2 spatial vectors. Compared with the number of spatial vectors of the SM system in (1), implying that QSM can transmit one more extra index bits of $\log_2 N_t$, namely the spectral efficiency in QSM system can be further improved when the two schemes (SM, QSM) transmit the modulated symbol with the same modulation order. In other words, QSM can achieve better bit error ratio (BER) performance since the QSM scheme transmits a data symbol of lower modulation order than the SM scheme at the same data rate.

Thus, the squared MED between the TSVs for the QSM system could be calculated by

$$d^2_{\mathbf{S}_{\mathrm{QSM}},\min} = \min_{\mathbf{S}_{\mathrm{QSM}} \neq \tilde{\mathbf{S}}_{\mathrm{QSM}}} \left\{ \left\| \mathbf{S}_{\mathrm{QSM}} - \tilde{\mathbf{S}}_{\mathrm{QSM}} \right\|^2 \right\} = \frac{2}{E_{\mathrm{av}}}. \quad (4)$$

Compared with the squared MED of SM, it can be seen from the formulas of both (2) and (4) that the squared MED of QSM is inferior to that of SM. Essentially, the squared MED of QSM is larger than that of SM at the same spectral efficiency. For example, let $N_t = 4$ and 8 bits/s/Hz for both SM and QSM, thus a 64QAM/PSK and 16QAM/PSK symbol are applied for SM and QSM, respectively. Hence, we have $d^2_{\mathbf{S}_{\mathrm{SM}},\min} = 4/42$ and $d^2_{\mathbf{S}_{\mathrm{QSM}},\min} = 2/10$.

In the next section, inspired by the core idea of both SM and QSM, we will introduce our proposed QIM-TDC scheme by exploiting the spatial and signal constellation domains for further improving the reliability of transmission.

III. DESIGN OF THE PROPOSED QIM-TDC SYSTEM

In this paper, we consider the QIM-TDC system with N_t TAs and N_r receive antennas. For the system model of QIM-TDC, as depicted in Fig. 3, a total number of incoming B data bits are conveyed by a 3D constellation modulator, an in-phase AI selector **A** including an in-phase AI set κ of activating two TAs and a quadrature AI selector **B** including a quadrature AI set **e** of activating only a single RF-chain TA. Furthermore, the X-axis, Y-axis and Z-axis components of the modulated 3D symbol are divided and then mapped on the corresponding active TAs by both the in-phase AI vector and the quadrature AI vector, as shown in the shadow box of Fig. 3.

In the transmitting module of Fig. 3, a TSV $\mathbf{S}_n \in \mathrm{C}^{N_t \times 1}$, $\mathbf{S}_n \in \{\mathbf{S}_1, \mathbf{S}_2, \cdots, \mathbf{S}_{2^B}\}$ is communicated with a receiver equipped by N_r receive antennas. The TSV constellation of QIM-TDC could be denoted as: the real spatial vector $\mathbf{S}_{\Re}$ of a TSV is comprised with both two components (X-axis and Y-axis) of the modulated 3D symbol and the index of two active TAs from which the two components are transmitted, and the imaginary vector $\mathbf{S}_{\Im}$ of the TSV is comprised with both the remaining one component (Z-axis) of the modulated

TABLE 2. EXAMPLES of QIM-TDC mapping rule, modulating a 3DC symbol $S(m_x, m_y, m_z)$ by AI information bits $[B_2, B_3] = [b_1, b_2, b_3, b_4]$ at one time slot into a TSV S.

$[B_2, B_3]$ bits		Antenna index vector	Antenna index vector	Real spatial vector	Imaginary spatial vector	Transmitted Spatial Vector
$[b_1, b_2]$	$[b_3, b_4]$	κ_i	$\mathbf{e}_k$	$\mathbf{S}_{\Re}$	$\mathbf{S}_{\Im}$	$\mathbf{S}$
00	00	$[1\,0\,1\,0]^T$	$[1\,0\,0\,0]^T$	$[m_x\ 0\ m_y\ 0]^T$	$[m_z\ 0\ 0\ 0]^T$	$[m_x + jm_z, 0, m_y, 0]^T$
00	01	$[1\,0\,1\,0]^T$	$[0\,1\,0\,0]^T$	$[m_x\ 0\ m_y\ 0]^T$	$[0\ m_z\ 0\ 0]^T$	$[m_x, jm_z, m_y, 0]^T$
01	10	$[1\,0\,0\,1]^T$	$[0\,0\,1\,0]^T$	$[m_x\ 0\ 0\ m_y]^T$	$[0\ 0\ m_z\ 0]^T$	$[m_x, 0, jm_z, m_y]^T$
01	11	$[1\,0\,0\,1]^T$	$[0\,0\,0\,1]^T$	$[m_x\ 0\ 0\ m_y]^T$	$[0\ 0\ 0\ m_z]^T$	$[m_x, 0, 0, m_y + jm_z]^T$
10	00	$[0\,1\,1\,0]^T$	$[1\,0\,0\,0]^T$	$[0\ m_x\ m_y\ 0]^T$	$[m_z\ 0\ 0\ 0]^T$	$[jm_z, m_x, m_y, 0]^T$
10	01	$[0\,1\,1\,0]^T$	$[0\,1\,0\,0]^T$	$[0\ m_x\ m_y\ 0]^T$	$[0\ m_z\ 0\ 0]^T$	$[0, m_x + jm_z, m_y, 0]^T$
11	10	$[0\,1\,0\,1]^T$	$[0\,0\,1\,0]^T$	$[0\ m_x\ 0\ m_y]^T$	$[0\ 0\ m_z\ 0]^T$	$[0, m_x, jm_z, m_y]^T$
11	11	$[0\,1\,0\,1]^T$	$[0\,0\,0\,1]^T$	$[0\ m_x\ 0\ m_y]^T$	$[0\ 0\ 0\ m_z]^T$	$[0, m_x, 0, m_y + jm_z]^T$

3D symbol and the index of only one active TA from which the remaining one component is transmitted.

Observed that the incoming B data bits are divided into three blocks by the bit stream splitter of Fig. 3. The first block of $B_1 = \log_2 N$ bits is fed into the 3D constellation modulator and modulated into a 3D symbol $S(m_x, m_y, m_z)$ from a N-ary constellation set Ω_S, the optimal design of which for the increasing of spatial gain will be introduced in the Section IV, where N denotes the number of CPs in designed 3D constellation. Then, considering that two out of N_t TAs are chosen by mapping B_2 bits to carry two components m_x, m_y of the resulting 3D symbol during the transmission, which results in the increasing of spatial diversity gain. Furthermore, one out of N_t TAs is chosen by mapping B_3 bits to carry the remaining one component m_z of the resulting 3D symbol during the transmission. Thus, three components of the modulated 3D symbol can be conveyed without interference each other.

In the module of the in-phase AI selector $\mathbf{A}$, an in-phase AI set κ consists of 2^{B_2} AI vectors, each of which includes two non-elements equaling to 1 for the activation of two TAs, and other zero-elements of the AI vector correspond to the unactivated TAs for the real spatial vector $\mathbf{S}_{\Re}$. Thus, the second block B_2, containing $\left\lfloor \log_2 C_{N_t}^2 \right\rfloor$ bits, is used for selecting an AI vector κ_i from the set of in-phase AI κ to activate two TAs, where C_x^y is the combination of operation and $\lfloor . \rfloor$ is the floor operation, the AI set $\kappa = \{\kappa_1, \kappa_2, \cdots, \kappa_i, \cdots, \kappa_{N_\alpha}\} \in \alpha$, $N_\alpha = 2^{\left\lfloor \log_2 C_{N_t}^2 \right\rfloor}$, α denotes the set that includes all possible combinations of activating two out of N_t TAs. Furthermore, the two active TAs activated by the AI vector κ_i are then used to respectively modulate two components m_x, m_y of the resulting 3D symbol, resulting in a spatial vector that is considered as the real $\mathbf{S}_{\Re}$ part of the TSV $\mathbf{S}$.

Similarly with the AI selector $\mathbf{A}$, in the quadrature AI selector $\mathbf{B}$, the last block of $B_3 = \log_2 N_t$ bits is used for selecting an AI vector $\mathbf{e}_k$ from the set of quadrature AI $\mathbf{e}$ to activate a single RF-chain TA. The AI vector $\mathbf{e}_k$ drawn from the set with the cardinality N_t

$$\mathbf{e} = \left\{\mathbf{e}_1, \mathbf{e}_2, \cdots, \mathbf{e}_k, \cdots, \mathbf{e}_{N_t}\right\}, \tag{5}$$

where $\mathbf{e}_k \in \mathbf{R}^{N_t}$, $k = 1, 2, \cdots, N_t$, is the k-th column of the $(N_t \times N_t)$-element identity matrix $\mathbf{I}_{N_t}$. In other words, only a single transmit antenna with index k is activated at each time slot. Then the activated single TA is used to modulate the component m_z of the resulting 3D symbol, resulting in a spatial vector that is considered as the imaginary $\mathbf{S}_{\Im}$ part of the TSV $\mathbf{S}$.

Consequently, by adding both the real spatial vector $\mathbf{S}_{\Re}$ and the imaginary spatial vector $\mathbf{S}_{\Im}$, the TSV can be expressed as

$$\mathbf{S} = \mathbf{S}_{\Re} + j\mathbf{S}_{\Im}, \tag{6}$$

Due to the transmit power follows $P = 1$, the normalized TSV $\bar{\mathbf{S}} = \frac{\mathbf{S}}{E_{\text{av}}^{3\text{D}}}$, where $E_{\text{av}}^{3\text{D}}$ denotes the average energy per TSV or per 3D CP.

To further explain the working principle of the proposed QIM-3DC scheme, EXAMPLEs of creating a TSV $\mathbf{S}$ are given in what follows. Assumed that $N_t = 4$, a modulated 3D constellation symbol $S(m_x, m_y, m_z)$, $[B_2, B_3] = [\underbrace{b_1, b_2}_{B_2}, \underbrace{b_3, b_4}_{B_3}]$ bits, $\kappa = \{[1\,0\,1\,0]^T, [1\,0\,0\,1]^T, [0\,1\,1\,0]^T, [0\,1\,0\,1]^T\}$, $\mathbf{e} = \{[1\,0\,0\,0]^T, [0\,1\,0\,0]^T, [0\,0\,1\,0]^T, [0\,0\,0\,1]^T\}$, where 0 and 1 denotes the off and on of the corresponding TA, respectively. The TSVs are generated as the results in Table 2.

At the receiver, the normalized received spatial signal vector is expressed as

$$\begin{aligned}\mathbf{Y} &= \mathbf{H} \cdot \bar{\mathbf{S}} + \mathbf{N} \\ &= \frac{1}{\sqrt{E_{\text{av}}^{3D}}} \cdot (\mathbf{h}_\xi^i \cdot m_x + \mathbf{h}_\psi^i \cdot m_y + j \cdot \mathbf{h}_k^k \cdot m_z) + \mathbf{N},\end{aligned} \tag{7}$$

where $\mathbf{Y} \in C^{N_r \times 1}$ is a receiver signal vector. The Rayleigh fading MIMO channel matrix $\mathbf{H} = \left[\mathbf{h}_1, \cdots, \cdots, \mathbf{h}_{N_t}\right] \in C^{N_r \times N_t}$ and the additive white Gaussian noise (AWGN) vector $\mathbf{N} \in C^{N_r \times 1}$, each entry of both is independent and identically distributed (i.i.d) complex-valued Gaussian random variables with $CN(0, 1)$ and $(0, \sigma_N^2)$, respectively. $\mathbf{h}_\xi^i, \mathbf{h}_\psi^i$ denote the ξ-th, ψ-th column vector of $\mathbf{H}$ corresponding to the i-th AI vector from the AI vector set κ, respectively. $\mathbf{h}_k^k$ denotes the k-th column vector of $\mathbf{H}$ corresponding to the k-th AI vector from the AI vector set $\mathbf{e}$. Note that $\xi \in \left\{1, \cdots, \frac{N_t}{2}\right\}$, $\psi \in \left\{1 + \frac{N_t}{2}, \cdots, N_t\right\}$.

Assuming that the perfect channel state information (CSI) can be retrieved at the receiver, the maximum likelihood (ML) decoder estimate three parameters: the in-phase AI i,

the quadrature AI k, and the 3D constellation symbol S. After detection of the ML decoder, which performs the exhaustive search among the whole TSVs, the estimated in-phase AI i, quadrature k and 3D symbol S are obtained by

$$\left[\hat{i}, \hat{k}, \hat{S}\right] = \arg\min_{i,k,S} \left\|\mathbf{Y} - \mathbf{H} \cdot \bar{\mathbf{S}}\right\|^2 \tag{8}$$

where $\hat{i}$, $\hat{k}$ denote the estimated in-phase and quadrature AI number. $\hat{S}$ denotes the estimated 3D constellation symbol.

IV. CONSTRUCTION OF THREE-DIMENSION CONSTELLATION

In single-input single-output (SISO) or single-input multi-output (SIMO) communication systems, the squared MED between the signal CPs plays a key role in the reliability performance of wireless communication systems at high signal noise ratio (SNR). Similarly, in MIMO system, the modulated QAM/PSK constellation symbols are mapped on the corresponding active TAs to form a TSV, and then transmitted to the receiving end. Hence, the squared MED between the TSVs plays a key role in the reliability performance of MIMO system. Since the different distribution of signal CP can effect the squared MED between the TSVs, to maximize the squared MED between the TSVs for the QIM-TDC scheme, we can optimize the distribution of signal CPs in 3D constellation according to the theory of the squared MED between the TSVs.

In this paper, based on the design of the proposed QIM-TDC scheme, the X-axis and Y-axis, Z-axis components of a 3D constellation symbol are modulated on the corresponding two active TAs in the in-phase dimension and one active TA in the quadrature dimension, respectively. Due to the difference between the original spatial AI bits and the evaluated spatial AI bits, the differences between the in-phase and quadrature AIes and the estimated in-phase and quadrature AIes result in that the unnormalized squared Euclidean distance $d_{\mathbf{s}}^2$ has following eight cases as (9), as shown at the bottom of this page. Furthermore, assumed a 3D constellation is constructed by both QAM and PAM constellation, we define that the signal CPs of both QAM and PAM constellation are $s_m^{\mathrm{Q}}(s_{m,\Re}^{\mathrm{Q}}, s_{m,\Im}^{\mathrm{Q}})$, $m \in \{1, \cdots, M\}$ and $s_l^{\mathrm{P}}, l \in \{1, \cdots, L\}$, respectively. M and L denote the number of CPs in both QAM and PAM constellation, respectively. According to the permutation of $s_{\Re}^{\mathrm{Q}}$, $s_{\Im}^{\mathrm{Q}}$, s^{P}, a 3D constellation may have six cases as following

$$S(m_x, m_y, m_z) \in \begin{cases} (s_{\Re}^{\mathrm{Q}}, s_{\Im}^{\mathrm{Q}}, s^{\mathrm{P}}) & \text{(a)} \\ (s_{\Re}^{\mathrm{Q}}, s^{\mathrm{P}}, s_{\Im}^{\mathrm{Q}}) & \text{(b)} \\ (s^{\mathrm{P}}, s_{\Re}^{\mathrm{Q}}, s_{\Im}^{\mathrm{Q}}) & \text{(c)} \\ (s^{\mathrm{P}}, s_{\Im}^{\mathrm{Q}}, s_{\Re}^{\mathrm{Q}}) & \text{(d)} \\ (s_{\Im}^{\mathrm{Q}}, s^{\mathrm{P}}, s_{\Re}^{\mathrm{Q}}) & \text{(e)} \\ (s_{\Im}^{\mathrm{Q}}, s_{\Re}^{\mathrm{Q}}, s^{\mathrm{P}}) & \text{(f).} \end{cases} \tag{10}$$

Thus, based on both (9) and (10), the squared MED between the TSVs may be calculated by

$$d_{\mathbf{S},\min}^2 = \min_{\mathbf{S} \neq \mathbf{S}'} \{\frac{\left\|\mathbf{S} - \mathbf{S}'\right\|^2}{E_{\mathrm{av}}^{3\mathrm{D}}}\}, \tag{11}$$

where

$$\begin{aligned} E_{\mathrm{av}}^{3\mathrm{D}} &= E_{\mathrm{av}}^{\mathrm{Q}} + E_{\mathrm{av}}^{\mathrm{P}} \\ &= \frac{1}{N}\sum_{n=1}^{N} S_n^2(m_x, m_y, m_z) \\ &= \frac{1}{N}\sum_{n=1}^{N}\left(\left|m_x^n\right|^2 + \left|m_y^n\right|^2 + \left|m_z^n\right|^2\right), \\ E_{\mathrm{av}}^{\mathrm{Q}} &= \frac{1}{M}\sum_{m=1}^{M} s_m^{\mathrm{Q}}, \\ E_{\mathrm{av}}^{\mathrm{P}} &= \frac{1}{L}\sum_{l=1}^{L} s_l^{\mathrm{P}}, \end{aligned} \tag{12}$$

Next, two types of 3D constellation will be designed for the proposed QIM-TDC scheme. First, a traditional 3D constellation is composed of three components from both the traditional QAM and the traditional PAM constellation. Furthermore, according to the theoretical characteristics of the squared MED between the TSVs, a modified 3D constellation for maximizing the squared MED is derived by three components from both the traditional QAM and the improved PAM constellation.

A. 3DCI DESIGN

In the traditional M-QAM constellation (e.g. 8-QAM, $s^{\mathrm{Q}} = \{(s_{\Re}^{\mathrm{Q}}, s_{\Im}^{\mathrm{Q}})\}$, $s_{\Re}^{\mathrm{Q}}$, $s_{\Im}^{\mathrm{Q}} \in \{\pm 1, \pm 3\}$) and the L-PAM constellation

$$d_{\mathbf{s}}^2 = \begin{cases} \left|m_x - \hat{m}_x\right|^2 + \left|m_y - \hat{m}_y\right|^2 + \left|m_z - \hat{m}_z\right|^2, \text{ if } (\xi = \hat{\xi}, \psi = \hat{\psi}, k = \hat{k}) \\ |m_x|^2 + \left|\hat{m}_x\right|^2 + \left|m_y - \hat{m}_y\right|^2 + \left|m_z - \hat{m}_z\right|^2, \text{ if } (\xi \neq \hat{\xi}, \psi = \hat{\psi}, k = \hat{k}) \\ \left|m_x - \hat{m}_x\right|^2 + \left|m_y\right|^2 + \left|\hat{m}_y\right|^2 + \left|m_z - \hat{m}_z\right|^2, \text{ if } (\xi = \hat{\xi}, \psi \neq \hat{\psi}, k = \hat{k}) \\ \left|m_x - \hat{m}_x\right|^2 + \left|m_y - \hat{m}_y\right|^2 + |m_z|^2 + \left|\hat{m}_z\right|^2, \text{ if } (\xi = \hat{\xi}, \psi = \hat{\psi}, k \neq \hat{k}) \\ |m_x|^2 + \left|\hat{m}_x\right|^2 + \left|m_y\right|^2 + \left|\hat{m}_y\right|^2 + \left|m_z - \hat{m}_z\right|^2, \text{ if } (\xi \neq \hat{\xi}, \psi \neq \hat{\psi}, k = \hat{k}) \\ |m_x|^2 + \left|\hat{m}_x\right|^2 + \left|m_y - \hat{m}_y\right|^2 + |m_z|^2 + \left|\hat{m}_z\right|^2, \text{ if } (\xi \neq \hat{\xi}, \psi = \hat{\psi}, k \neq \hat{k}) \\ \left|m_x - \hat{m}_x\right|^2 + \left|m_y\right|^2 + \left|\hat{m}_y\right|^2 + |m_z|^2 + \left|\hat{m}_z\right|^2, \text{ if } (\xi = \hat{\xi}, \psi \neq \hat{\psi}, k \neq \hat{k}) \\ |m_x|^2 + \left|\hat{m}_x\right|^2 + \left|m_y\right|^2 + \left|\hat{m}_y\right|^2 + |m_z|^2 + \left|\hat{m}_z\right|^2, \text{ if } (\xi \neq \hat{\xi}, \psi \neq \hat{\psi}, k \neq \hat{k}) \end{cases} \tag{9}$$

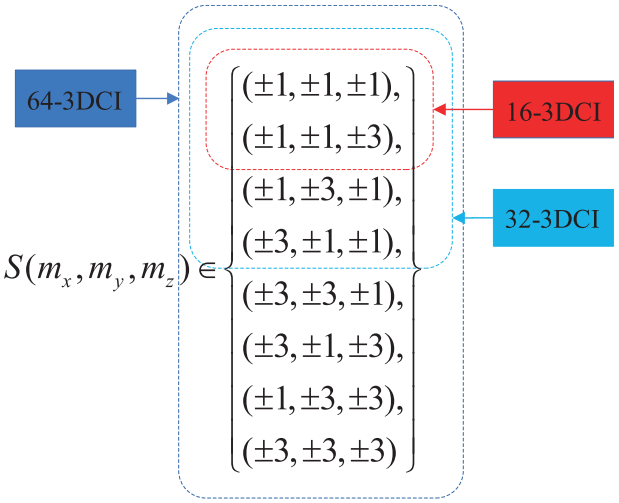

FIGURE 4. 16-,32-,64-ary 3DCI.

(e.g. 2-PAM, $s^{\mathrm{P}} = \{\pm1\}$), the range of values for the real $s^{\mathrm{Q}}_{\Re}$ and imaginary $s^{\mathrm{Q}}_{\Im}$ of s^{Q} and s^{P} are given as

$$s^{\mathrm{Q}}_{\Re}, s^{\mathrm{Q}}_{\Im}, s^{\mathrm{P}} \in \{\pm1, \pm3, \cdots, \pm[2(\tau-1)+1], \tau \in Z\}, \quad (13)$$

where Z denotes integer field.

Through three values of $s^{\mathrm{Q}}_{\Re}, s^{\mathrm{Q}}_{\Im}, s^{\mathrm{P}}$, a 3D constellation is directly constructed, named as 3DCI, and may be designed as

1) $M = 2, L = 2$

In this case of both $M = 2$ and $L = 2$, we can design an 8-ary 3DCI constellation when considering $s^{\mathrm{Q}}_{\Re}, s^{\mathrm{Q}}_{\Im}, s^{\mathrm{P}} \in \{\pm1\}$. Although there are six cases by (10) for a 3DCI constellation, each 3D constellation generated by each of the six cases has the same 3D CPs due to the same range values. Hence, only one case in (10) is considered to be designed for a 3D constellation. For this case, an 8-ary 3DCI constellation can be designed as

$$S(m_x, m_y, m_z) \in \{(\pm1, \pm1, \pm1)\} \quad (14)$$

2) $M = 4, L = 4$

In this case of both $M = 4$ and $L = 4$, we can design the higher order 3DCI constellations, such as $N = 16, 32, 64$ when considering $s^{\mathrm{Q}}_{\Re}, s^{\mathrm{Q}}_{\Im}, s^{\mathrm{P}} \in \{\pm1, \pm3\}$.

Since $s^{\mathrm{Q}}_{\Re}, s^{\mathrm{Q}}_{\Im}, s^{\mathrm{P}}$ have four states: $(\pm1, \pm3)$, by six cases in (10), $s^{\mathrm{Q}}_{\Re}, s^{\mathrm{Q}}_{\Im}, s^{\mathrm{P}}$ may generate the $C^1_4 \cdot C^1_4 \cdot C^1_4 \times 6$ of 3D CPs. Note that $s^{\mathrm{Q}}_{\Re}, s^{\mathrm{Q}}_{\Im}, s^{\mathrm{P}}$ for each case of (10) are combined to generate the $C^1_4 \cdot C^1_4 \cdot C^1_4$ of 3D CPs that is the same as the $C^1_4 \cdot C^1_4 \cdot C^1_4$ of 3D CPs obtained by other cases in (10). Hence, we may design $C^1_4 \cdot C^1_4 \cdot C^1_4$ of 3D CPs at most, as depicted in Fig. 4.

Thus, we can select some CPs from $C^1_4 \cdot C^1_4 \cdot C^1_4$ of 3D CPs in Fig. 4 to design N-ary 3D constellation of modulation order $N = 16, 32, 64$. Taking the relationship of both the squared MED between adjacent CPs and the average energy of each CP in 3DCI constellation into account, it can be seen from Fig. 4 that the 3D CPs in red box are considered for 16-3DCI, the 3D CPs in the light blue box are considered for 32-3DCI, and the 3D CPs in the dark blue box are considered for 64-3DCI.

In brief, the higher-order 3D constellations are constructed by the range value of $s^{\mathrm{Q}}_{\Re}, s^{\mathrm{Q}}_{\Im}, s^{\mathrm{P}}$ in (13).

According to the working principle of the proposed QIM-TDC scheme, after modulating the 3DCI symbol on the corresponding active TAs in both in-phase and quadrature dimensions and then forming a TSV symbol, the squared MED between the TSVs based on (9) and (11) are derived as (15) in the three cases of $\xi \neq \hat{\xi}, \psi = \hat{\psi}, k = \hat{k}$ and $\xi = \hat{\xi}, \psi \neq \hat{\psi}, k = \hat{k}$ and $\xi = \hat{\xi}, \psi = \hat{\psi}, k \neq \hat{k}$ in (9),

$$\begin{aligned} d^2_{\mathbf{S},\min} &= \min_{\mathbf{S}\neq\mathbf{S}'} \{\frac{\|\mathbf{S}-\mathbf{S}'\|^2}{E^{3\mathrm{D}}_{\mathrm{av}}}\} \\ &= \min\left\{\frac{2\left|s^{\mathrm{Q}}_{\Re}\right|^2}{E^{3\mathrm{D}}_{\mathrm{av}}}, \frac{2\left|s^{\mathrm{Q}}_{\Im}\right|^2}{E^{3\mathrm{D}}_{\mathrm{av}}}, \frac{2\left|s^{\mathrm{P}}\right|^2}{E^{3\mathrm{D}}_{\mathrm{av}}}\right\} \\ &= \frac{2}{E^{3\mathrm{D}}_{\mathrm{av}}}(\min\{\left|s^{\mathrm{Q}}_{\Re}\right|\} = \min\{\left|s^{\mathrm{Q}}_{\Im}\right|\} = \min\{\left|s^{\mathrm{P}}\right|\} = 1), \end{aligned} \quad (15)$$

For example, for a 16-3DCI $S(m_x, m_y, m_z) \in \{(\pm1, \pm1, \pm1), (\pm1, \pm1, \pm3)\}$, $E^{3\mathrm{D}}_{\mathrm{av}} = 7$, $d^2_{\bar{\mathbf{S}},\min} = 2/7$.

B. 3DCII DESIGN

At high signal noise ratio (SNR), to a certain extent, the BEP performance of the MIMO wireless communication system can be improved by maximizing the squared MED between the TSVs. Based on the analysis described in the above subsection, we note that the squared MED of (15) is inversely proportional to the average energy $E^{3\mathrm{D}}_{\mathrm{av}}$ of each CPs when the 3D constellation is applied for the QIM-TDC system. In this subsection, abiding by the rule of both eight cases in (9) and the squared MED between the TSVs in (15), a new 3D constellation, which is the extension of 3DCI constellation, named as 3DCII, is constructed to maximize the squared MED between the TSVs for the better reliability of transmission. In other words, on condition that the squared MED between the adjacent 3DCII symbols is equal to the squared MED between the TSVs, the average energy $E^{3\mathrm{D}}_{\mathrm{av}}$ can be reduced by designing m_x or m_y or m_z value of some CPs in 3D constellation when the modulation order N of the designed 3DCII constellation is the same as that of the 3DCI constellation.

Hence, the key idea of designing a new 3DCII constellation is to increase the squared MED $d^2_{\bar{\mathbf{S}},\min}$ by reducing the average energy $E^{3\mathrm{D}}_{\mathrm{av}}$. We define the CP symbol $\tilde{S}(\tilde{m}_x, \tilde{m}_y, \tilde{m}_z) = \tilde{S}(\tilde{s}^{\mathrm{Q}}_{\Re}, \tilde{s}^{\mathrm{Q}}_{\Re}, \tilde{s}^{\mathrm{P}})$ in 3DCII constellation.

Combining the six cases of (10) with the squared Euclidean distance $d^2_{\mathbf{S},\min}$ between the TSVs in (9), when

the 3DCII constellation is applied for the QIM-TDC system, the squared MED $d^2_{\tilde{\mathbf{S}},\min}$ between the TSVs may be given by

$$d^2_{\tilde{\mathbf{S}},\min} = \begin{cases} \min\left\{\dfrac{2a^2}{\tilde{E}^{3D}_{av}}, \dfrac{2b^2}{\tilde{E}^{3D}_{av}}, \dfrac{2c^2}{\tilde{E}^{3D}_{av}}\right\}, & (\kappa_1) \\ \min\left\{\dfrac{2\left|\tilde{s}^{Q}_{\Re}\right|^2}{\tilde{E}^{3D}_{av}}, \dfrac{2\left|\tilde{s}^{Q}_{\Im}\right|^2}{\tilde{E}^{3D}_{av}}, \dfrac{2\left|\tilde{s}^{P}\right|^2}{\tilde{E}^{3D}_{av}}\right\}, & (\kappa_2), \end{cases} \tag{16}$$

where $a = \left|\tilde{s}^{Q}_{\Re} - \tilde{s}^{P}\right|, b = \left|\tilde{s}^{Q}_{\Im} - \tilde{s}^{P}\right|, c = \left|\tilde{s}^{Q}_{\Im} - \tilde{s}^{Q}_{\Re}\right|$. $\tilde{E}^{3D}_{av}$ denotes the average energy of each CP in 3DCII constellation. $\kappa_1 = (\xi = \hat{\xi}, \psi = \hat{\psi}, k = \hat{k})$ denotes that all groups of AI bits are correctly detected at the receiver, $\kappa_2 = (\xi \neq \hat{\xi}, \psi = \hat{\psi}, k = \hat{k})$ or $(\xi = \hat{\xi}, \psi \neq \hat{\psi}, k = \hat{k})$ or $(\xi = \hat{\xi}, \psi = \hat{\psi}, k \neq \hat{k})$ denotes that only one group of AI bits is detected incorrectly.

In this paper, the real and imaginary part $s^{Q}_{\Re}, s^{Q}_{\Im}$ of the conventional M-QAM are considered as two components (X-axis, Y-axis) of $\tilde{S}(\tilde{m}_x, \tilde{m}_y, \tilde{m}_z)$ in the 3DCII constellation. In this case, after obtaining a 3DCII constellation and mapping it into a TSV vector, abiding by the rule of the squared MED between the TSVs in (15), the formula of (16) can be rewritten as

$$d^2_{\tilde{\mathbf{S}},\min} = \begin{cases} \left\{\dfrac{\min\left\{2a^2\right\}}{\tilde{E}^{3D}_{av}}, \dfrac{\min\left\{2b^2\right\}}{\tilde{E}^{3D}_{av}}\right\}, & (\kappa_1) \\ \left\{\dfrac{2}{\tilde{E}^{3D}_{av}}, \dfrac{\min\left\{2\left|\tilde{s}^{P}\right|^2\right\}}{\tilde{E}^{3D}_{av}}\right\}, & (\kappa_2). \end{cases} \tag{17}$$

Thus, according to the design idea of the squared MED between the adjacent 3DCII symbols is equal to the squared MED between the TSVs and abiding by the rule of the squared MED $\frac{2}{\tilde{E}^{3D}_{av}}$ between the TSVs in (15), the problem of designing the CPs $\tilde{S}(\tilde{m}_x, \tilde{m}_y, \tilde{m}_z)$ in the 3DCII constellation for maximizing the squared MED can be formulated as (18) when considering the unnormalization of CP in 3DCII constellation.

$$d^2_{s} = \begin{cases} \min\left\{2\left|s^{Q}_{\Re} - \tilde{s}^{P}\right|^2\right\} = 2, \\ \min\left\{2\left|s^{Q}_{\Im} - \tilde{s}^{P}\right|^2\right\} = 2, \\ \min\left\{2\left|\tilde{s}^{P}\right|^2\right\} \geq 2. \end{cases} \tag{18}$$

Obviously, when two components (X-axis and Y-axis) of the designed 3DCII constellation $\tilde{S}(\tilde{m}_x, \tilde{m}_y, \tilde{m}_z)$ are determined from the given M-QAM constellation. Due to the derivation of (18), the PAM constellation for the remain one component (Z-axis) of $\tilde{S}(\tilde{m}_x, \tilde{m}_y, \tilde{m}_z)$ may be designed as

$$\tilde{s}^{P} \in \left\{\pm 2, \pm 4, \cdots, 2\tau', \tau' \in Z\right\}, \tag{19}$$

where Z denotes integer field.

Then, with the aid of both $s^{Q}_{\Re}$ and $s^{Q}_{\Im}$ from M-QAM constellation and $\tilde{s}^{P}$ in the above mentioned (19), the N-ary 3DCII symbol $\tilde{S}(\tilde{m}_x, \tilde{m}_y, \tilde{m}_z)$ can be designed as

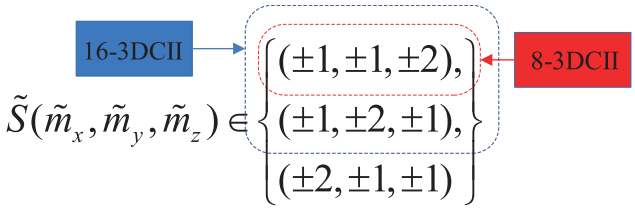

FIGURE 5. 8-, 16-ary 3DCII.

1) $M = 2, L = 2$

In this case of both $M = 2$ and $L = 2$, we can design two N-3DCII constellations of modulation order $N = 8, 16$ when considering that $s^{Q}_{\Re}, s^{Q}_{\Im} \in \{\pm 1\}$ and $\tilde{s}^{P} \in \{\pm 2\}$.

Since $s^{Q}_{\Re}, s^{Q}_{\Im}$ have the same range values and are different from that of $\tilde{s}^{P}$, such that the 3DCII constellation constructed by the first three cases (a, b, c) of (10) are the same as that constructed by the last three cases (d, e, f) of (10). Thus, we can design $C^1_2 \cdot C^1_2 \cdot C^1_2 \cdot 3$ type of CPs, as depicted in Fig. 5.

Consequently, the 3D CPs in red box of Fig. 5 may be considered for 8-3DCII, it has $\tilde{E}^{3D}_{av} = 6$, $d^2_{\tilde{\mathbf{S}},\min} = 2/6$. However, $E^{3D}_{av} = 3$, $d^2_{\tilde{\mathbf{S}},\min} = 2/3$ in 8-3DCI constellation. In this case, the 8-3DCI constellation is considered for the proposed QIM-TDC scheme, rather than the 8-3DCII constellation. Then, the 3D CPs for 16-3DCII in the dark blue box of Fig. 5 may be considered. Because of $\tilde{E}^{3D}_{av} = 6$, thus $d^2_{\tilde{\mathbf{S}},\min} = 2/6$ is greater than $d^2_{\tilde{\mathbf{S}},\min} = 2/7$ obtained by 16-3DCI constellation.

2) $M = 4, L = 2$

Accordingly to the six cases of (10), in this case of both $M = 4$ and $L = 2$, we can design the $C^1_4 \cdot C^1_4 \cdot C^1_2 \cdot 3$ of CPs when $s^{Q}_{\Re}, s^{Q}_{\Im} \in \{\pm 1, \pm 3\}$ and $\tilde{s}^{P} \in \{\pm 2\}$, as depicted in Fig. 6. Due to the minimizing of the average energy per 3D CP, such that two N-3DCII constellations of high modulation order $N = 32, 64$ may be designed as the virtual frames (the CPs in the red box for 32-3DCII, the CPs in the black blue box for 64-3DCII) in Fig. 6.

Based on the above mentioned analysis and (11), the squared MED between the TSVs obtained by mapping a 3D symbol $\tilde{S}(\tilde{m}_x, \tilde{m}_y, \tilde{m}_z)$ on the active TAs in the in-phase and quadrature dimensions may be calculated by

$$d^2_{\tilde{\mathbf{S}},\min} \underset{\mathbf{S}\neq\mathbf{S}'}{=} \min\{\frac{\left\|\mathbf{S} - \mathbf{S}'\right\|^2}{\tilde{E}^{3D}_{av}}\} = \frac{2}{\tilde{E}^{3D}_{av}}. \tag{20}$$

where $\tilde{E}^{3D}_{av} = \frac{1}{N}\sum_{n=1}^{N}\left(\left|\tilde{m}^n_x\right|^2 + \left|\tilde{m}^n_y\right|^2 + \left|\tilde{m}^n_z\right|^2\right)$.

For example, for a 32-3DCII CPs shown in red box of Fig. 6, $\tilde{E}^{3D}_{av} = 8$, which is less than $E^{3D}_{av} = 9$ obtained by 32-3DCI constellation.

V. PERFORMANCE ANALYSIS

In this section, the squared MED between the TSVs and an upper bound of the average BEP performances are analyzed

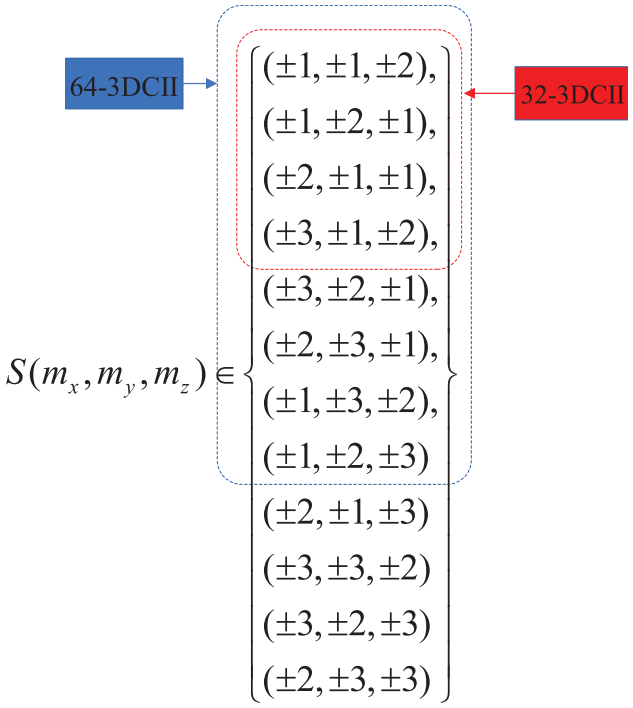

FIGURE 6. 32-, 64-ary 3DCII.

TABLE 3. Comparison of the squared MED between QIM-TDC with various MIMO schemes at different spectral efficiency for both the number of TAs $N_t = 4$ and $N_t = 8$.

	4TX7b	4TX8b	4TX10b	4TX11b
SM [2]	4/20	4/42	4/170	4/330
QSM [4]	0.2929	2/10	2/42	2/82
ESM [16]	–	4/11.5	4/28.5	4/51.75
QIM-TDCI	2/3	2/7	2/15	2/23.5
QIM-TDCII	2/6	2/6	2/11	2/16.25
	8TX10b	8TX11b	8TX12b	8TX13b
SM [2]	4/82	4/170	4/330	4/682
QSM [4]	2/10	2/20	2/42	2/82
ESM [16]	4/11.5	–	4/26.5	4/47.875
QIM-TDCI	2/3	2/7	2/9	2/15
QIM-TDCII	2/6	2/6	2/8	2/11

to demonstrate the outstanding performances of the proposed QIM-TDC scheme.

A. SQUARED MINIMUM EUCLIDEAN DISTANCE

At high SNR, the asymptotic performance is mainly determined by the worst-case PEP, which corresponds to the squared MED between the TSVs. By comprehensive considering these equations including (11), (15), and (20), the squared MEDs $d^2_{\bar{\mathbf{S}},\min}$ of the QIM-TDC scheme with both 3DCI and 3DCII (named as QIM-TDCI and QIM-TDCII) are listed in Table 3 and compared with that of various MIMO schemes such as SM, QSM, ESM at different spectral efficiencies.

It can be observed from Table 3 that the squared MED $d^2_{\bar{\mathbf{S}},\min}$ between the TSVs generated by both the proposed QIM-TDCI and QIM-TDCII schemes have the larger value than that generated by other MIMO schemes (e.g. SM, QSM, ESM) at the same spectral efficiency except that the squared MED $d^2_{\bar{\mathbf{S}},\min}$ of QIM-TDCI at both 4TX8b and 4TX10b and of QIM-TDCII at 4TX8b have a little modesty compared with that of the ESM scheme.

Hence, in high SNR region, the performance of the presented QIM-TDC scheme using the proper constellation is more reliable than other MIMO schemes in wireless communication network except for the case of 4TX8b.

In Table 3, note that p_1TXp_2b denotes transmitting p_2 bits in one time slot with p_1 TAs. That is, a TSV can carry the number of information bits at one time slot. For each scheme, the corresponding modulation order can be derived by $M = 2^{(p_2 - I^{\alpha}_{\mathrm{AI}})}$, where I^{α}_{AI} denotes the total number of antenna index bits in the α scheme. For example, in this case of $N_t = 4$, it has $I^{\alpha}_{\mathrm{AI}} = 4$ bits for all schemes. In this case of $N_t = 8$, the antenna index bits are $I^{\mathrm{SM}}_{\mathrm{AI}} = 3$ bits, $I^{\mathrm{QSM}}_{\mathrm{AI}} = 6$ bits, $I^{\mathrm{ESM}}_{\mathrm{AI}} = 6$ bits, $I^{\mathrm{QIM-TDC}}_{\mathrm{AI}} = 7$ bits, respectively.

For the case of the worst-case PEP, it can be deduced from the Table 3 that the code gain of the proposed QIM-TDC scheme over that of other MIMO schemes can be evaluated by the ratio of the squared MED between two different schemes, as follows

$$\begin{aligned} G &= 10\log_{10}\left(\frac{d^2_{\bar{\mathbf{S}}^{\mathrm{QIM-TDC}},\min}}{d^2_{\bar{\mathbf{S}}^{x},\min}}\right) \\ &= 10\log_{10}\left(\frac{E^{x}_{\mathrm{av}}}{\varepsilon \cdot E^{\mathrm{QIM-TDC}}_{\mathrm{av}}}\right), \end{aligned} \tag{21}$$

where $d^2_{\bar{\mathbf{S}}^{x},\min}$ denotes the squared MED of the x scheme, the value of ε is the molecular ratio between the squared MED formulas in MIMO schemes.

For example, the expected code gain of the QIM-TDC scheme over that of the QSM scheme in the scenario of 8TX10b is calculated by

$$G = 10\log_{10}\left(\frac{2/3}{2/10}\right) = 5.2288 \text{ dB} \tag{22}$$

The above mentioned data analyses demonstrate the outstanding performances of the proposed QIM-TDC scheme in application for the MIMO system.

B. AVERAGE BEP ANALYSIS OF THE QIM-TDC SCHEME

With the assumption of perfect CSI, the estimated vector symbol of the normalized TSV $\bar{\mathbf{S}}$ is expressed as $\hat{\bar{\mathbf{S}}}$, the pairwise error probability (PEP) conditioned on $\mathbf{H}$ can be calculated by

$$P\left(\bar{\mathbf{S}} \to \hat{\bar{\mathbf{S}}} \middle| \mathbf{H}\right) = Q\left(\sqrt{\frac{1}{2\sigma^2} \cdot \left\|\mathbf{H} \cdot \left(\bar{\mathbf{S}} - \hat{\bar{\mathbf{S}}}\right)\right\|^2}\right), \tag{23}$$

where $Q(\cdot)$ denotes the Gaussian Q function, $Q(x) = \frac{1}{\pi}\int_0^{\frac{\pi}{2}} \exp\left(\frac{-x^2}{2\sin^2\theta}\right) d\theta$.

Using a moment generating function (MGF) from [19], the average PEP is given by

$$\begin{aligned}\bar{P}\left(\bar{\mathbf{S}} \to \hat{\bar{\mathbf{S}}}\right) &= \frac{1}{\pi} E_{\mathbf{H}} \left\{ \int_0^{\frac{\pi}{2}} \exp\left(\frac{-\left\| \mathbf{H} \cdot \left(\bar{\mathbf{S}} - \hat{\bar{\mathbf{S}}}\right) \right\|^2}{4\sigma^2 \cdot \sin^2\theta} \right) d\theta \right\} \\ &= \left(\frac{1-\eta}{2}\right)^{N_r} \sum_{r=0}^{N_r-1} \binom{N_r - 1 + k}{r} \left(\frac{1+\eta}{2}\right)^r, \quad (24)\end{aligned}$$

where $\eta = \sqrt{\frac{\bar{\gamma}}{1+\bar{\gamma}}}$, $\bar{\gamma} = \frac{d_{\bar{\mathbf{S}}}^2}{4\sigma^2}$, the Euclidean distance $d_{\bar{\mathbf{S}}}^2 = \frac{d_{\bar{\mathbf{S}}}^2}{E_{\text{av}}^{3\text{D}}}$ ($\frac{d_{\bar{\mathbf{S}}}^2}{\bar{E}_{\text{av}}^{3\text{D}}}$) can be calculated out by (9).

Thus, an upper bound on the average BEP for the QIM-TDC scheme based on the union bound technique [19] can be derived as

$$P_b \le \frac{1}{B2^B} \sum_{v=1}^{2^B} \sum_{w=1}^{2^B} P\left(\bar{\mathbf{S}}_v \to \hat{\bar{\mathbf{S}}}_w\right) \cdot e\left(\bar{\mathbf{S}}_v \to \hat{\bar{\mathbf{S}}}_w\right) \quad (25)$$

where $e\left(\bar{\mathbf{S}}_v \to \hat{\bar{\mathbf{S}}}_w\right)$ is the total number of erroneous bits associated with the corresponding PEP event.

Comprehensively considering (9), (11), (24) and (25), since the worse PEP is mainly determined by the squared MED $d_{\bar{\mathbf{S}},\min}^2$ at high SNR region, the more the squared MED $d_{\bar{\mathbf{S}},\min}^2$ is maximized, the smaller the average PEP value in (24). Such that the lower average BEP in (25) is achieved.

VI. NUMERICAL RESULTS AND DISCUSSIONS

In this section, based on the analysis of Table 3, the average BER (namely, BEP) performances of the QIM-TDC scheme with both the conventional 3D constellation and the modified 3D constellation are characterized with Monte Carlo simulation results over AWGN and Rayleigh fading channels. We also compare the BER of our presented QIM-TDC with that of other MIMO schemes such as SM, QSM, DSM and ESM, when the same parameters in MIMO system are configured.

In both Fig. 7 and Fig. 8, the average BER results of theoretic analysis (the green, black, purple, cyan curve) are compared with the simulated BER results (the blue, red curve) in scenarios of 4TX7b,4TX8b, 4TX10b and 4TX11b when $N_r = 4$, and of 8TX10b, 8TX11b, 8TX12b and 8TX13b when $N_r = 8$. Note that $p_1\text{TX}p_2\text{b}$ which has been introduced in the above section denotes $p2$ information bits are transmitted through the number of $p1$ TAs at each time slot. It can be observed that our derived BER curve at high SNR matches well with the simulated BER curve. It verifies the effectiveness of our proposed QIM-TDC scheme.

Fig. 9 presents the average BER performance for the two scenarios of both 4TX7b and 4TX8b. Based on the analysis of the squared MED $d_{\bar{\mathbf{S}},\min}^2$ in Table 3, $d_{\bar{\mathbf{S}},\min}^2$ of QIM-TDC using 16-3DCII has a slightly inferior to that of ESM using 16QAM for the case of 4TX8b, namely it has a gap of

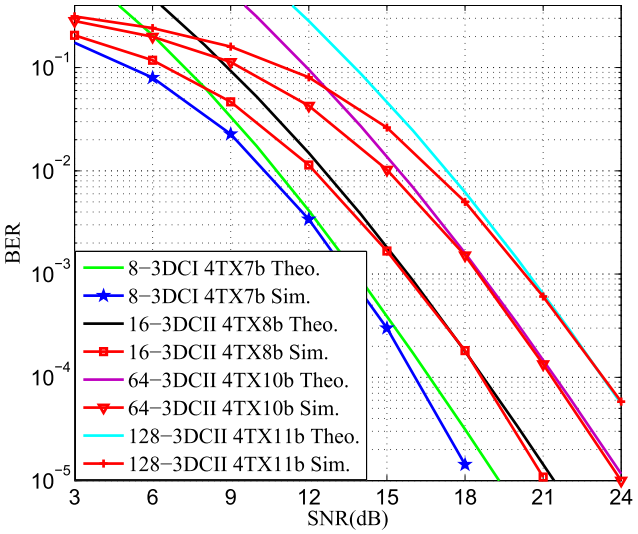

FIGURE 7. The analytical and simulation results of the average BER curve versus SNR for QIM-TDC with the scenarios of 4TX7b,4TX8b, 4TX10b and 4TX11b when $N_r = 4$.

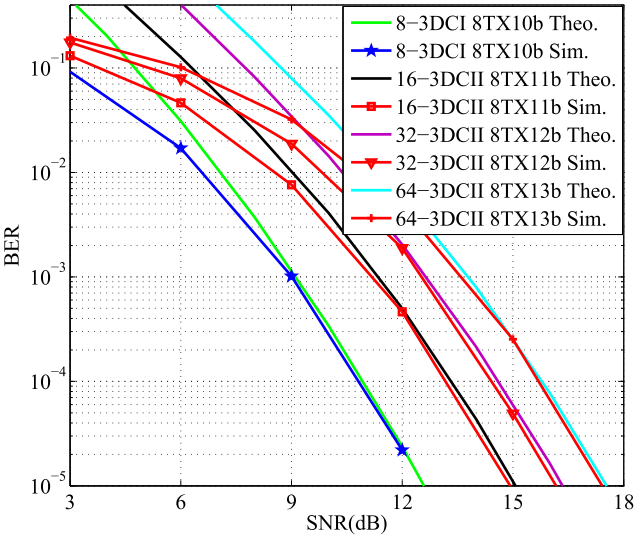

FIGURE 8. The analytical and simulation results of the average BER curve versus SNR for QIM-TDC with the scenarios of 8TX10b,8TX11b, 8TX12b and 8TX13b when $N_r = 8$.

the theoretical $G = 10\log_{10}\left(\frac{2/6}{4/11.5}\right)$ SNR gains according to (21). Observed from Fig. 9 that the better SNR gains for the proposed QIM-TDC scheme are achieved as compared with other MIMO schemes such as the SM, QSM schemes. Especially, the QIM-TDC scheme using 8-3DCI outperforms 5 dB SNR gains over the SM scheme using 32QAM, and approximately 2.5 dB SNR gains over the QSM scheme using 8PSK at the BER value of 10^{-4} for the scenario of 4TX7b. And for the scenario of 4TX8b, the QIM-TDC scheme (such as the red curve) is slightly inferior to the ESM scheme at the high SNR region.

In Fig. 10, for this case of 4TX10b, we compare the BER performance of the presented QIM-TDC using 64-ary CPs with that of other MIMO schemes, including the SM scheme

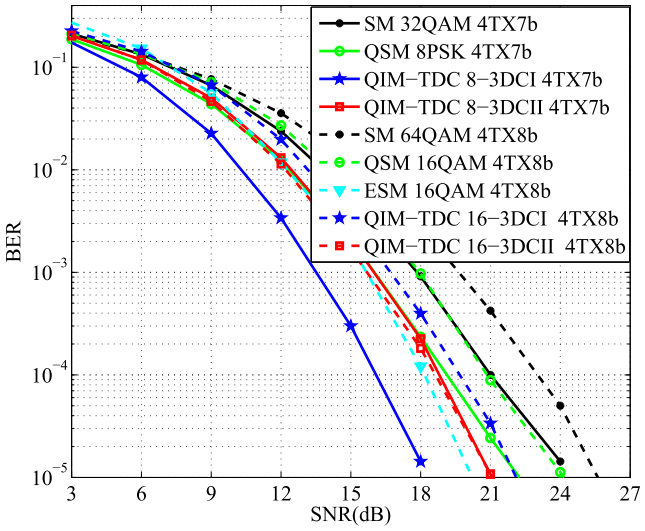

FIGURE 9. BER performance comparison between QIM-TDC and other schemes such as SM, QSM ESM at both the real curve for 4TX7b and the virtual curve for 4TX8b when $N_r = 4$.

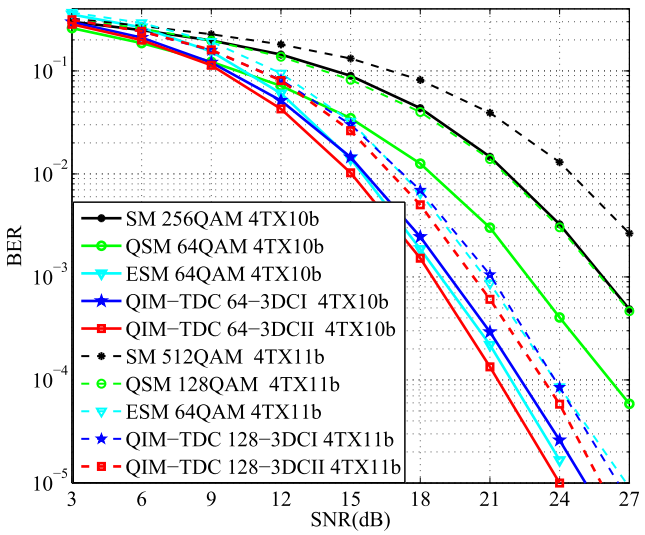

FIGURE 10. BER performance comparison between QIM-TDC and other schemes such as SM, QSM ESM at both the real curve for 4TX10b and the virtual curve for 4TX11b when $N_r = 4$.

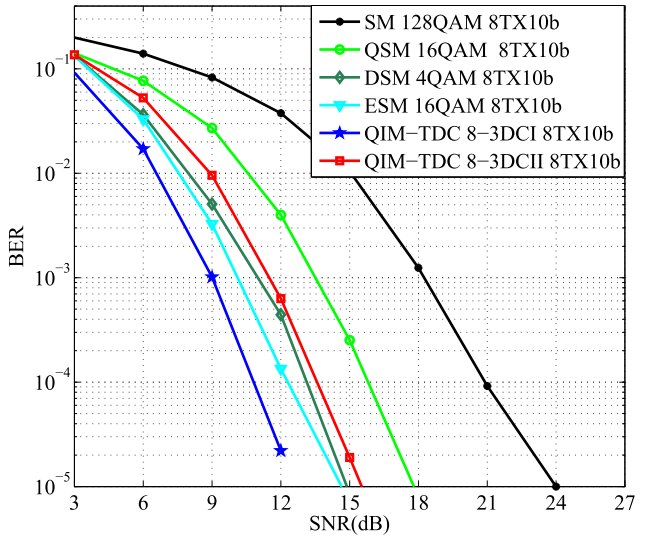

FIGURE 11. BER performance comparison between QIM-TDC and other schemes such as SM, QSM, DSM, ESM for the case of 8TX10b.

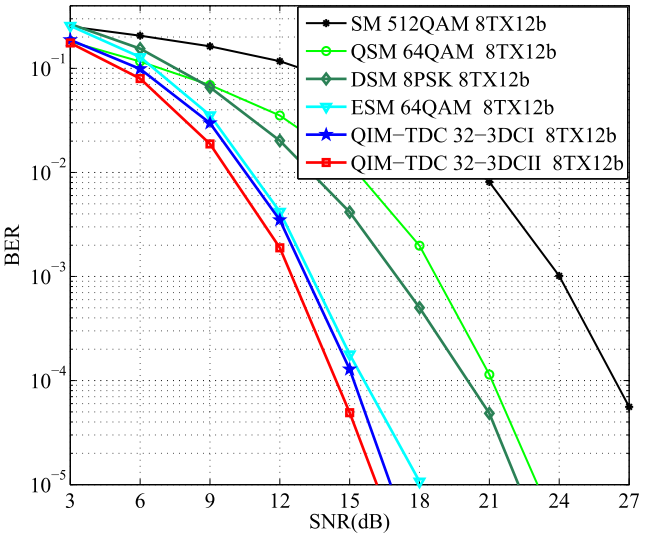

FIGURE 12. BER performance comparison between QIM-TDC and other schemes such as SM, QSM, DSM, ESM for the case of 8TX12b.

with 256QAM and the QSM scheme with 64QAM, the ESM scheme with 64QAM. Based on the analysis of both Table 3 and (21), the ideal code gains of QIM-TDC using 64-3DCII over that of SM is 8.88 dB SNR gains, over that of QSM is 5.81 dB SNR gains, and over that of ESM is 1.12 dB SNR gains at the higher SNR region. In the scenario of 4TX10b, observed from Fig. 10 that approximately 7 dB SNR gains over the SM scheme, 4.2 dB over the QSM scheme and 0.5 dB over the ESM scheme at BER value of 10^{-3} are achieved for the QIM-TDC scheme with 64-3DCII. Since the squared MED $d^2_{\tilde{\mathbf{S}},\min}$ of QIM-TDC using 64-3DCI is inferior to that of ESM, its BER performance is a slightly 0.22 dB SNR gain less than that of ESM by (21). Furthermore, the dot simulation curves for 4TX11b show that the presented QIM-TDC using 128-3DCII has the better BER performance as compared with other MIMO schemes such as SM using 512QAM, QSM using 128QAM, ESM using 64QAM due to the maximizing of the squared MED $d^2_{\tilde{\mathbf{S}},\min}$. Note that QIM-TDC with 128-3DCI also has a little better BER performance than ESM at the higher SNR region. Hence, these simulation results demonstrate the effectiveness of our theory derivation.

When the same spectral efficiency is configured with the number of TAs $N_t = 8$, due to the achieving of more AI bits of the QIM-TDC scheme than other MIMO schemes, the QIM-TDC scheme employs the constellation symbols that have lower modulation order. Hence, the squared MED $d^2_{\tilde{\mathbf{S}},\min}$ of the QIM-TDC system is the bigger than that of other schemes. Consequently, in the scenario of 8TX10b shown

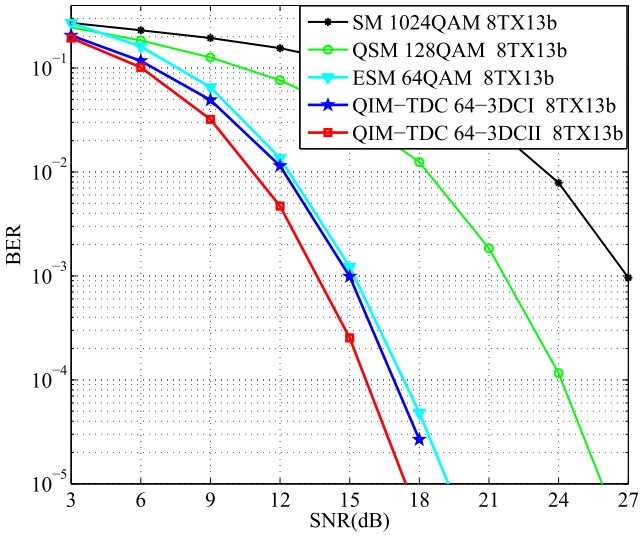

FIGURE 13. BER performance comparison between QIM-TDC and other schemes such as SM, QSM ESM for the case of 8TX13b.

in Fig. 11, it could be observed that the average BER performance of the QIM-TDC scheme with 8-3DCI outperforms approximately 10.5 dB, 5 dB, 2.2 dB, 1.6dB SNR gains over that of SM, QSM, DSM, ESM at BER value of 10^{-4}, respectively. The QIM-TDC scheme with 8-3DCII also achieves approximately 7.5 dB SNR gains over SM, 2 dB SNR gains over QSM, respectively. Nonetheless, observed from Fig. 11 that it is inferior to both DSM and ESM based on the analysis of both Table 3 and (21).

From Fig. 12 and Fig. 13, it could be observed that the QIM-TDC scheme with two 3D constellations achieves better BER performance than other MIMO schemes due to the maximization of the squared MED between TSVs and the transmission of more additional AI bits.

Therefore, based on the analysis of the above mentioned schemes of constellation design, 8-ary 3DCI and N-ary 3DCII ($N \geq 16$) are the best candidate for the proposed QIM-TDC system. Further exploiting the spatial domain from the TAs and the signal domain from the signal constellation, the better average BER performance of the QIM-TDC system can be achieved than that of the other schemes such as SM, QSM, DSM and ESM. Such that the spatial and signal constellation domains in MIMO system are worth of further investigating and exploiting.

VII. CONCLUSION

In this paper, we present a new scheme of QIM-TDC structure to further exploit the spatial domain in order to enhance the reliability of the MIMO-based communication system. A 3D constellation symbol is conveyed by the proposed QIM-TDC system. Then, a modified 3D constellation is designed to maximize the squared MED between the TSVs, such that the BEP performance of our presented scheme has been improved. Furthermore, the squared MED and the BEP performance are analyzed and showed the advantage of the QIM-TDC system. Finally, the numerical analysis results demonstrate that our presented scheme improves the BEP performance of the MIMO-based communication system than that of other MIMO-based systems (e.g., SM, QSM, DSM, ESM) by exploiting the spatial and signal constellation domains of the TAs.

REFERENCES

[1] E. Basar, M. Wen, R. Mesleh, M. Di Renzo, Y. Xiao, and H. Haas, "Index modulation techniques for next-generation wireless networks," *IEEE Access*, vol. 5, pp. 16693–16746, 2017.
[2] R. Y. Mesleh, H. Haas, S. Sinanovic, C. W. Ahn, and S. Yun, "Spatial modulation," *IEEE Trans. Veh. Technol.*, vol. 57, no. 4, pp. 2228–2241, Jul. 2008.
[3] M. Di Renzo, H. Haas, A. Ghrayeb, S. Sugiura, and L. Hanzo, "Spatial modulation for generalized MIMO: Challenges, opportunities, and implementation," in *Proc. IEEE Int. Conf. Wireless Commun. Signal (WCSP)*, Jan. 2014, pp. 56–103.
[4] R. Mesleh, S. S. Ikki, and H. M. Aggoune, "Quadrature spatial modulation," *IEEE Trans. Veh. Technol.*, vol. 64, no. 6, pp. 2738–2742, Jun. 2015.
[5] A. Younis, N. Serafimovski, R. Mesleh, and H. Haas, "Generalised spatial modulation," in *Proc. Asilomar Conf. Signals, Syst., Comput.*, Pacific Grove, CA, USA, Nov. 2010, pp. 1498–1502.
[6] T. Datta and A. Chockalingam, "On generalized spatial modulation," in *Proc. IEEE Wireless Commun. Netw. Conf. (WCNC)*, Shanghai, China, Apr. 2013, pp. 2716–2721.
[7] J. Fu, C. Hou, W. Xiang, L. Yan, and Y. Hou, "Generalised spatial modulation with multiple active transmit antennas," in *Proc. IEEE Globecom Workshops*, Miami, FL, USA, Dec. 2010, pp. 839–844.
[8] J. Wang, S. Jia, and J. Song, "Generalised spatial modulation system with multiple active transmit antennas and low complexity detection scheme," *IEEE Trans. Wireless Commun.*, vol. 11, no. 4, pp. 1605–1615, Apr. 2012.
[9] T. Datta, H. S. Eshwaraiah, and A. Chockalingam, "Generalized space-and-frequency index modulation," *IEEE Trans. Veh. Technol.*, vol. 65, no. 7, pp. 4911–4924, Jul. 2016.
[10] Z. Yigit and E. Basar, "Double spatial modulation: A high-rate index modulation scheme for MIMO systems," in *Proc. Int. Symp. Wireless Commun. Syst. (ISWCS)*, Poznan, Poland, Sep. 2016, pp. 347–351.
[11] P. Yang, Y. Xiao, B. Zhang, S. Li, M. El-Hajjar, and L. Hanzo, "Star-QAM signaling constellations for spatial modulation," *IEEE Trans. Veh. Technol.*, vol. 63, no. 8, pp. 3741–3749, Oct. 2014.
[12] P. Zhang, C. Wang, S. Guo, and H. Zhang, "Novel APM constellation design for spatial modulation systems," in *Proc. Int. Conf. Wireless Commun. Signal Process. (WCSP)*, Nanjing, China, Oct. 2015, pp. 1–5.
[13] M. Maleki, H. R. Bahrami, S. Beygi, M. Kafashan, and N. H. Tran, "Space modulation with CSI: Constellation design and performance evaluation," *IEEE Trans. Veh. Technol.*, vol. 62, no. 4, pp. 1623–1634, May 2013.
[14] M. Maleki, H. R. Bahrami, and A. Alizadeh, "Constellation design for spatial modulation," in *Proc. IEEE Int. Conf. Commun. (ICC)*, London, U.K., Jun. 2015, pp. 2739–2743.
[15] B. T. Vo, H. H. Nguyen, and H. D. Tuan, "Constellation design for quadrature spatial modulation," in *Proc. IEEE 86th Veh. Technol. Conf.*, Toronto, ON, Canada, Sep. 2017, pp. 1–5.
[16] C.-C. Cheng, H. Sari, S. Sezginer, and Y. T. Su, "Enhanced spatial modulation with multiple signal constellations," *IEEE Trans. Commun.*, vol. 63, no. 6, pp. 2237–2248, Jun. 2015.
[17] C.-C. Cheng, H. Sari, S. Sezginer, and Y. T. Su, "New signal designs for enhanced spatial modulation," *IEEE Trans. Wireless Commun.*, vol. 15, no. 11, pp. 7766–7777, Nov. 2016.
[18] P. W. Wolniansky, G. J. Foschini, G. D. Golden, and R. A. Valenzuela, "V-BLAST: An architecture for realizing very high data rates over the rich-scattering wireless channel," in *Proc. URSI Int. Symp. Signals, Syst., Electron. Conf.*, Pisa, Italy, Oct. 1998, pp. 295–300.
[19] M. K. Simon and M. Alouini, *Digital Communication Over Fading Channels* (Wiley Series in Telecommunications and Signal Processing), 2nd ed. Hoboken, NJ, USA: Wiley, 2005.

FUCHUN HUANG received the B.E. degree in electronics information engineering from Henan Polytechnic University, China, in 2008, and the M.E. degree in telecommunication and information system from Jiangsu University, China, in 2012. He is currently pursuing the Ph.D. degree with the School of Electronic and Information Engineering, Sun Yat-sen University, Guangzhou, China. He is currently with the Department of Computer, South China Institute of Software Engineering, Guangzhou. His current research interests include index modulation, spatial constellation design, antenna selection algorithms, and OFDM.

XUEHUA LIU received the B.E. degree in electronics information engineering from Huanggang Normal University, China, in 2006, and the M.E. degree in computer technology from the Wuhan University of Technology, China, in 2012. She is currently with the Department of Computer, South China Institute of Software Engineering, Guangzhou, China. Her current research interests include the IoT communication technology and wireless communication.

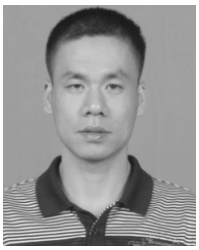

ZHILI ZHOU received the B.S. degree in automation engineering and the M.S. degree in communication and information system from the Zhejiang University of Technology, China, in 2001 and 2009, respectively, and the Ph.D. degree in communication engineering from Sun Yat-sen University, China, in 2018. He is currently with the College of Electrical and Electronic Engineering, Wenzhou University. His research interests include signal processing and artificial intelligence.

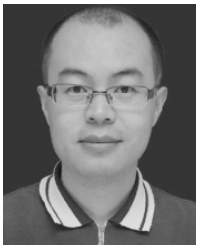

JIABING LUO received the B.E. degree in medicinal botany from Northwestern University, China, in 1998, and the M.E. degree in computer application technology from the Guangdong University of Technology, China, in 2007. He is currently with the Department of Computer, South China Institute of Software Engineering, Guangzhou, China. His current research interests include the IoT communication technology, automation control, embedded technology, and deep learning.

JILIN WANG received the B.E. degree in education technology from Huber Normal University, China, in 2007, and the M.E. degree in education technology from Huazhong Normal University, China, in 2014. She is currently with the Department of Computer, South China Institute of Software Engineering, Guangzhou, China. Her current research interests include artificial intelligence and mobile learning.